

PACS numbers: 52.25.Os; 52.50.Jm; 52.38.Mf
DOI: 10.1070/QE2006v036n05ABEH013243

Percolation and emission spectra of a laser plasma upon ablation of silicon and silicon-containing composites

N.E. Kask, S.V. Michurin, G.M. Fedorov

***Abstract*. The emission spectra of plasmas produced near the surface of silicon and sulphur samples and their mixtures by nanosecond and millisecond laser pulses are studied in a broad range of pressures of buffer gases. The percolation dependences are obtained for composite Si–S, Si–SiO_2, and SiO_2–S targets. It is found that experimental percolation thresholds coincide with the typical threshold for three-dimensional continual percolation.**

Keywords: *laser ablation, laser plasma, percolation.*

1. Introduction

Synthesis of nanoscale structures with controllable parameters and their self-assembling into larger structures with unique properties and functions is a fundamental direction in modern science. The solution of this problem is of interest for many branches of science such as physics, chemistry, biology, materials technology, nanoelectronics, and computation engineering. One of the promising methods for producing nanostructures is laser ablation, which allows one to synthesise nanostructures for a variety of materials. The combination of laser ablation, which is used for producing the vapour–gas phase of the target material, and the vapour–liquid–solid (VLS) method of crystal growth already allows the fabrication of macroscopic amounts of single crystal nanowires made of various materials, including doped semiconductors [1]. Pulsed laser ablation has a number of advantages over conventional methods for preparing nanoparticles, in particular, the possibility of producing monodisperse clusters with a narrow size distribution [2].

The dynamics of plasma expansion into a surrounding gas, the plasma composition and various processes proceeding in it such as absorption of laser radiation, heating, ionisation, recombination, condensation and clustering depend, in particular, on the external pressure produced by the surrounding gas. According to [3], at pressures lower than 10^{-5} atm, a free adiabatic expansion of the plasma takes place. Upon ablation of aluminium [3] and silicon [4] targets, it follows from the relation between the intensities of ion lines that the plasma temperature achieves its maximum ($\sim 10^4$ K) by the single-pulse end and then decreases with the characteristic time $\sim 10^{-7}$ s.

Initially, associates (dimers, trimers, etc.) are formed in a laser plume. In the case of the effusion method, their concentration with respect to that of monomers can amount to 0.1 [5]. As shown in papers [4, 6], nanoparticles are absent at low pressures ($P < 10^{-4}$ atm) of the surrounding gas. Collisions of plasma particles with atoms of the surrounding (buffer) gas become noticeable at pressures $\sim 10^{-4}$ atm; this is accompanied by a noticeable increase in the plasma plume emission within $1 - 2$ μs after the end of a laser pulse.

It is obvious that the increase in the plasma emission observed after a few microseconds during plasma expansion into the surrounding gas is caused by the change in its emission (absorption) ability. It is also known from experiments [4, 7] that the intensity of discrete spectral lines and molecular bands belonging to ions and dimmers of the evaporated material, respectively, correlates with the efficiency of formation of condensate nanoparticles. Ions are centres of heterogeneous nucleation: vapour atoms polarised in the ion field are attracted to them [4]. According to [8], dimers are the main unit in gas-like clusters.

During the time of the order of 10^{-4} s, compact clusters containing $10^3 - 10^4$ atoms appear in the cooled layers of a vapour–gas flow due to vapour condensation and coagulation of the seeds of a liquid phase [6]. In the pressure range $(5 - 15) \times 10^{-4}$ atm, nanoclusters of size ~ 10 nm appear, which aggregate to form fractal clusters of size ~ 1 μm with increasing pressure up to $10^{-2} - 10^{-1}$ atm and restricting the expansion of the ablation cloud. Fractal clusters are observed within $\sim 10^{-2}$ s after irradiation by a millisecond laser pulse with a power density of $10^6 - 10^7$ W cm^{-2} [9]. Fractal aggregates are assembled into filament macrostructures in an external electric field. In experiments [9], fractal filaments appeared within $10^2 - 10^3$ s after the laser pulse action.

The mechanism of formation of macrostructures different from aggregation is realised, probably, upon a longer laser action and a correspondingly higher density of finely divided fraction in the laser plume. Thus, when the laser pulse duration was increased by a factor of ten, macrostructures appeared during the time $\sim 10^{-2}$ s even in the absence of an external field [10, 11]. It is assumed that the formation of macrostructures is triggered in this case by a percolation transition in a cluster of microfractals. Note that the threshold density of percolating particles depends on their shape, decreasing substantially with deviation from a

N.E. Kask, S.V. Michurin, G.M. Fedorov D.V. Skobel'tsyn Institute of Nuclear Physics, M.V. Lomonosov Moscow State University, Vorob'evy gory, 119992 Moscow, Russia; e-mail: nek@srd.sinp.msu.ru

Received 28 December 2005; revision received 18 April 2006
Kvantovaya Elektronika **36** (5) 435–439 (2006)
Translated by M.N. Sapozhnikov

spherical shape [12] and due to formation of linear nanostructures such as chains, nanowires, etc. It is known [1] that upon laser ablation of a silicon target containing a proper metal impurity, aside from nanoclusters, nanowires can be formed by the VLS mechanism [13], according to which a crystal nanowire grows in the region of its contact with a liquid drop being replenished, in turn, by atoms of a saturated vapour. The size of a drop representing the alloy of the target material with the metal determines the wire diameter, which always proves to be smaller than the drop diameter. Nanowires can be also formed by different mechanisms. Thus, upon ablation of a silicon target doped with silica, a silicon monoxide layer is formed at the intermediate stage [14], on which crystal silicon nanowires appear and grow. The efficiency of this process is maximal when the weight fractions of components (silicon and silica) in the target are equal.

It is interesting to study the percolation model in the case of efficient formation of reduced-dimensionality nanostructures in dense optical-discharge plasmas. According to this model, the so-called critical cluster of 'infinite' length is formed in a medium at the percolation threshold. The size of the nodes and branches of the percolation cluster produced in the vapour–gas region depend on the ratio of the rates of nucleation and growth of elementary geometrical objects – compact and molecular clusters, as a rule, of the nanometre scale. It can be expected that the thickness of branches of the percolation cluster will by of the atomic size in the limit.

Previous investigations [15, 16] have shown that the plasma produced upon ablation of targets into the surrounding gas by millisecond and nanosecond laser pulses contains three-dimensional percolation structures. The percolation threshold is the critical atomic density of the evaporated component of the target.

The dependence of the percolation threshold on the electronic structure of target atoms indicates to the presence of the chemical bond between structural elements of the percolation cluster [17]. Atoms and ions of the target material entering percolation structures do not contribute to the intensity of the corresponding discrete spectrum. As a result, the intensity of the discrete spectrum is not proportional to the density of the evaporated target component [16].

In this paper, we study the manifestation of percolation in emission spectra of plasmas depending on the buffer gas pressure and the composition of targets containing silicon. The studies were performed using laser pulses of different durations.

2. Experimental setup

Because the scheme of laser ablation experiments is quite universal and the setup used here was described in [18], we consider only the experimental parameters relevant to the solution of the problems formulated in the paper.

We used 1.06-μm laser pulses of different durations: (1) a 10-ns, 1-mJ single pulse from an LTIPCh-8 laser; (2) a train of ten 100-ns, 1-mJ pulses from a laser with a saturable filter; and (3) a quasi-continuous 10-ms, 100-J pulse. Experiments with different interaction times allowed us to reveal both general properties and specific features typical for the time scale and laser radiation density.

Laser radiation was focused into a spot of diameter ~ 1 mm on the target surface by a spherical lens with the focal distance $f = 30$ cm. The target (silicon and sulphur crystals and their pressed powder mixtures) was placed into a sealed chamber in which pressure could be varied from 0.001 to 150 atm.

We studied the spectra and emission intensity of the ablation cloud in the direction perpendicular to heating laser radiation. In the case of nanosecond pulses, the region of a laser plume under study was located at a distance of 500 μm from the target surface. The emission of a laser plume produced by quasi-continuous radiation was studied in regions located from the target at distances $d_1 = 5.5$ mm and $d_2 = 17.5$ mm.

3. Experimental results

3.1 Effect of pressure on the light flash spectrum

It was found in [18] that upon laser-induced evaporation of most metals, the laser plume emission intensity drastically increases by a few orders of magnitude at some external pressure P_{tr}, whose value is mainly determined by the target material. Such a critical behaviour, which is typical for the percolation transition, is also observed for some other characteristics of the plasma plume.

The study of the formation efficiency of fractal nanostructures showed [18] that at the threshold pressure of the surrounding gas, the energy of interaction between particles of the disperse phase in the laser plasma becomes equal to their kinetic energy. As a result, a disordered macroscopic fractal structure appears in external plasma layers already during laser irradiation. This is accompanied by an increase in the absorption and emission ability of the plasma and also in the effective colour temperature describing the spectral continuum of the light flash. The correlation of variations in the optical properties of plasma with the percolation threshold suggests that the spectral continuum of the laser plasma is related to the formation of percolation structures. According to [16], the increase in the continuum intensity is accompanied by the decrease in the intensity of discrete atomic spectra. Of interest are the dependences of the threshold pressure and emission spectra of the plasma on the laser pulse duration and power.

Figures 1 and 2 illustrate the behaviour of the spectral characteristics of the laser plasma produced near the silicon surface irradiated by laser pulses of different durations. The dependences of the intensity of spectral lines of silicon and emission continuum of the plasma on the buffer gas pressure are presented in the spectral range from 4000 to 6500 Å. Upon target ablation by nanosecond laser pulses, the emission spectra contain, along with continuum and buffer-gas lines, distinct doublet lines $4128 - 4131$ Å, $5056 - 5041$ Å, and $6347 - 6371$ Å belonging to singly ionised silicon ions.

Figure 1 compares the pressure dependences of the integrated intensity of the $4128 - 4131$ Å doublet and the continuum intensity obtained upon ablation of a Si target by nanosecond laser pulses with power densities 10^8 W cm^{-2} (single pulse) and 10^7 W cm^{-2} (pulse train). A buffer gas was helium. Figure 2 presents similar dependences in the case of plasma expansion in the argon atmosphere upon irradiation of the Si and S targets by a train of 10^7 W cm^{-2} pulses. In the case of a quasi-continuous 10^6 W cm^{-2} pulse, the increase in the continuum intensity is observed at the same pressures ($1 - 3$ atm) as upon irradiation by nano-

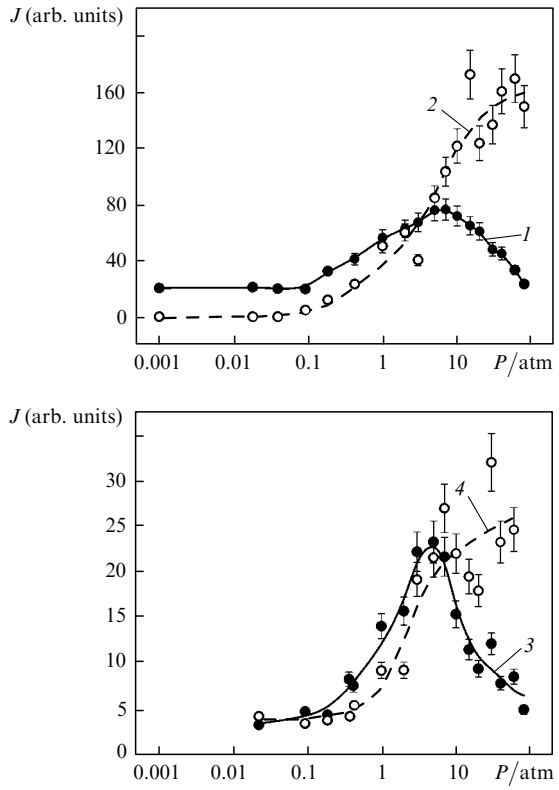

Figure 1. Dependences of the plasma emission intensity on pressure upon ablation of the Si target by a train of nanosecond pulses (*1, 2*) and a single pulse (*3, 4*) (buffer gas is helium): (*1, 3*) emission spectrum of silicon ions; (*2, 4*) continuum.

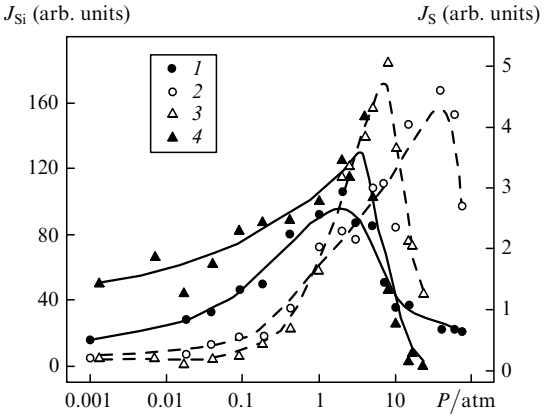

Figure 2. Dependences of the plasma emission intensity on pressure upon ablation of the Si (*1, 2*) and S (*3, 4*) targets by a train of nanosecond pulses (buffer gas is argon): (*1*) emission spectrum of silicon ions; (*2, 3*) continuum; (*4*) emission spectrum of sulphur ions.

second pulses; however, the behaviour of discrete spectra is different.

At comparatively low buffer-gas pressures ($\leqslant 1$ atm), the emission spectrum of the plasma does not contain the lines corresponding to silicon ions. The critical pressure at which the ion spectrum appears almost coincides in the case of a low radiation density with the threshold percolation pressure $P_{cr} \approx 1$ atm, above which the plasma temperature and continuum intensity begin to increase noticeably.

As follows from our previous studies [15–18], both the appearance of the continuum and population of high excited states at such a low radiation power density as 10^6 W cm^{-2} are related to the formation of percolation structures. Inside and in the periphery of a percolation cluster, giant fluctuations in the light-field strength are possible (up to 10^6 times) [19]. This leads to a noticeable difference between the electron and gas temperatures [18] and to the ionisation and excitation of high-energy levels (above 10 eV) of atoms, in particular, buffer-gas atoms (Ar, He). Silicon atoms and ions inside compact and percolation clusters do not contribute to discrete spectra.

As the surrounding gas pressure and plasma density are increased, a smaller part of target atoms remain in a free state, and a continuum (thermal emission of percolation structures) begins to dominate in the plasma emission. The threshold pressure at which the spectral characteristics of the plasma change almost does not depend on the laser pulse duration and laser power density. Note that the continuum intensity is mainly determined by hot clusters, which are formed within one–two microseconds after the action of short laser pulses [4].

Similar investigations were performed for plasmas produced upon ablation of polycrystalline sulphur targets. The results were similar to those obtained for silicon. In particular, upon irradiation by nanosecond pulses, the discrete spectrum consists only of the lines belonging to singly ionised sulphur ions. Figure 2 presents the dependences of the integrated intensity of the 5454 – 5474 Å doublet and continuum intensity of the buffer-gas (Ar) pressure obtained upon ablation of sulphur by a train of nanosecond pulses. No plasma emission was observed upon irradiation of polycrystalline sulphur by a 10-ms, 10^6 W cm^{-2} pulse.

3.2 Effect of the target composition on the light flash spectrum. Percolation upon ablation of the Si–S, $Si-SiO_2$, and SiO_2-S composites

Figures 3–5 present the dependences of the integrated intensities of discrete lines of the SiII and SII ions on the target composition upon ablation of binary targets made of powder Si–S, $Si-SiO_2$, and SiO_2-S composites by a train of nanosecond pulses. On the abscissa the relative density n_i of the number of silicon atoms (ions) in the plasma is plotted. The value of n_i was calculated assuming that the weight ratio of the components does not change during evaporation. In the case of a binary mixture of elements, the expression

$$n_i = [1 + (1 - x_i)\,\mu_i/(x_i\mu_j)]^{-1} \qquad (1)$$

is valid, where μ_i are the molecular weights of Si and S, and x_i are their weight fractions. Note that the relative density of the number of sulphur atoms is $n_j = 1 - n_i$.

As follows from the results presented in Fig. 3, at the initial stage the density of silicon and sulphur ions increases proportionally to the increase in the number of their atoms. The density of the number of ions in the plasma ceases to increase after the relative concentration of Si and S atoms in the target achieves threshold values:

$$N_{cr}(\mathrm{Si}) = 0.11 \pm 0.02, \quad N_{cr}(\mathrm{S}) = 0.20 \pm 0.04. \qquad (2)$$

The experimental thresholds for Si and S well agree with the value 0.15, which is typical for the threshold of three-

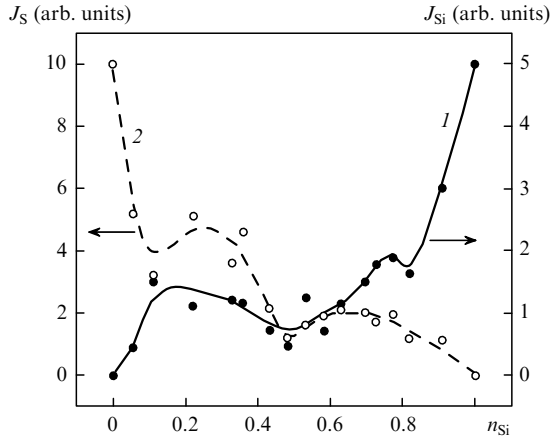

Figure 3. Dependences of the intensity of discrete emission spectra of silicon (*1*) and sulphur (*2*) on the composition of the Si – S composite (buffer gas is helium, $P = 1$ atm).

dimensional continual percolation in its potential model [20, 21]. After the target composition achieves the threshold for the second component, the density of the number of ions of the second component drastically increases. Upon ablation of targets with the composition lying between the two thresholds for S and Si, two percolation clusters consisting of silicon and sulphur atoms, respectively, exist in the plasma. Outside the above-mentioned interval, where the cluster of one of the components is absent, the ion concentration of another component in the plasma tends to the concentration existing near the surface of a single-component target. It is obvious that the mutual penetration of percolation clusters prevents the free flying apart of atoms and ions: atoms of the same kind in the dense plasma cannot overcome the energy barrier produced by particles of another kind.

Figure 4 shows the intensity of the emission lines of silicon on the composition of a $Si - SiO_2$ composite. Note that we have failed to identify discrete lines unambiguously belonging to silicon in the wavelength range under study. The analysis of dependences obtained upon ablation of the composite by nanosecond laser pulses presented in Fig. 4 gives the critical densities

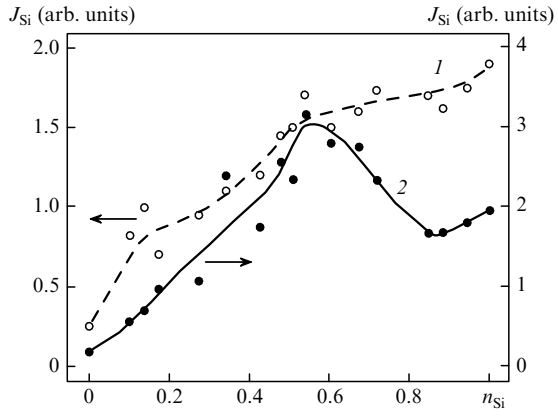

Figure 4. Dependences of the intensity of discrete emission spectra of silicon on the composition of the $Si - SO_2$ composite (buffer gas is helium, $P = 1$ atm): (*1*) single pulse; (*2*) train of nanosecond pulses.

$$N_{cr}(Si) = 0.15 \pm 0.02, \quad N_{cr}(SiO_2) = 0.14 \pm 0.02. \qquad (3)$$

When the relative concentration of Si atoms is $N_{cr}(Si)$, the initial increase in the intensity of silicon lines ceases, and, vice versa, for $N(Si) = 1 - N_{cr}(SiO_2)$, the intensity of silicon lines begins to increase, which is similar to the dependences for the Si–S composite. The abscissa for this composite is calculated from (1), where μ_j and n_j are the molecular weight and density of the number of silica molecules, respectively. Upon dissociation of silica molecules, the intermediate intensity maximum of the discrete spectrum of ions appears at the density $N(Si) \approx 0.5$.

Figure 5 presents the dependences of the line intensities on the composition of the $SiO_2 - S$ composite. By using (1) and the weight fractions of components for the characteristic points of these dependences, we obtained the critical densities of the target components $N_{cr}(SiO_2) = 0.14\pm 0.03$ and $N_{cr}(S) = 0.35 \pm 0.04$. Silicon atoms and ions appear upon laser ablation of this mixture only due to the dissociation of silica molecules. The presence of free oxygen atoms and molecules in the plasma reduces the relative densities of S and Si. By assuming a complete dissociation of silica molecules in the calculation of densities of silicon or sulphur ions, the first or second term in the right-hand side of expression (1) should be multiplied by three. By analysing the dependences presented in Fig. 5, we obtain

$$N_{cr}(Si) = 0.13 \pm 0.03, \quad N_{cr}(S) = 0.14 \pm 0.02. \qquad (4)$$

At these values, the initial increase in the intensity of spectral lines of the corresponding component ceases, and as in the case of the S–Si composite, vice versa, the intensity of spectral lines of the second component begins to increase.

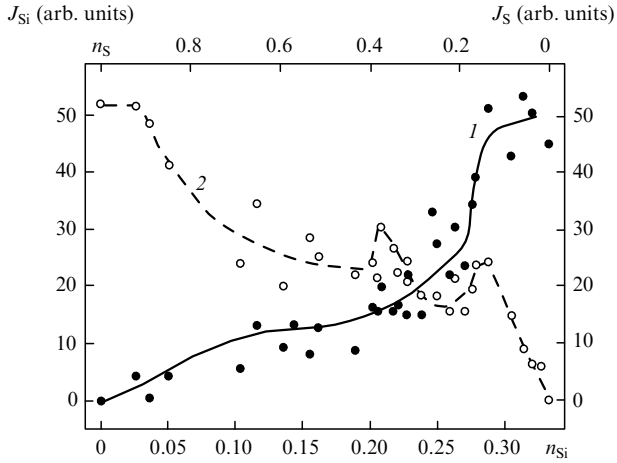

Figure 5. Dependences of the intensity of discrete emission spectra of silicon (*1*) and sulphur (*2*) on the composition of the $SiO_2 - S$ composite (buffer gas is helium, $P = 1$ atm).

Note that, if a target consists of a powder mixture, it can be also treated as a medium with three-dimensional percolation. However, the threshold in such an object is determined by the relative fraction of volumes of mixed components rather than by the atomic density [22]. In this case, according to the model of overlapping spheres, the characteristic percolation threshold p_v is ~ 0.3, which does

not correspond to experimental results (2)–(4) and dependences presented in Figs 3–5.

4. Conclusions

We have shown in this paper that upon ablation of targets into a surrounding gas by laser pulses of different durations, percolation in the plasma is manifested in emission spectra upon variations of the target composition and buffer-gas pressure. The percolation threshold is the critical atomic density of the evaporated target material. Good agreement between the critical densities for components of an individual composite and for different composites and between them demonstrates the validity of the percolation model for interpreting the results.

Acknowledgements. This work was supported by the Russian Foundation for Basic Research (Grant Nos 03-02-17026 and NSh-1771.2003.2).

References

1. Morales A.M., Lieber Ch.M. *Science*, **279**, 208 (1998).
2. Koshizaki N., Narazaki A., Sasaki T. *Scripta Mater.*, **44**, 1925 (1991).
3. Harilal S.S, Bindhu C.V., Tillack M.S., et al. *J. Appl. Phys.*, **93**, 2380 (2003).
4. Tillack M.S., Blair D.W., Harilal S.S. *Nanotechnol.*, **15**, 390 (2004).
5. Sidorov L.N., Korobov M.V., Zhuravleva L.V. *Mass-spektral'nye termodinamicheskie issledovaniya* (Mass Spectroscopy Thermodynamic Studies) (Moscow: Moscow State University, 1985).
6. Li Q., Sasaki T., Koshizaki N. *Appl. Phys.*, **69**, 115 (1999).
7. Arepalli S., Nicolaev P., Holmes W., Scott C.D. *Appl. Phys. A*, **70**, 125 (1999).
8. Zhukovitskii D.I. *Zh. Eksp. Teor. Fiz.*, **113**, 181 (1998).
9. Lushnikov A.A., Nechin A.E., Pakhomov A.V., Smirnov B.M. *Usp. Fiz. Nauk*, **161**, 113 (1991).
10. Kask N.E., Fedorov G.M. *Kvantovaya Elektron.*, **20**, 527 (1993) [*Quantum Electron.*, **23**, 453 (1993)].
11. Kask N.E., Fedorov G.M. *Vestn. Mosk. Univ., Ser. Fiz. Astron.*, (6), 25 (1998).
12. Bag A.L.R., Safran S.A., Webman I. *Phys. Rev. Lett.*, **54**, 1412 (1985).
13. Givargizov E.I *Rost nitevidnykh i plastinchatykh kristallov iz para* (Growth of Whisker and Scaly Crystals from Vapour) (Moscow: Nauka, 1977).
14. Lee S.T., Wang N., Lee C.S. *Mater. Sci. Eng.*, **A286**, 16 (2000).
15. Kask N.E., Michurin S.V., Fedorov G.M. *Zh. Eksp. Teor. Fiz.*, **116**, 1979 (1999).
16. Kask N.E., Michurin S.V., Fedorov G.M. *Kvantovaya Elektron.*, **35**, 48 (2005) [*Quantum Electron.*, **35**, 48 (2005)].
17. Kask N.E., Michurin S.V., Fedorov G.M. *Kvantovaya Elektron.*, **34**, 524 (2004) [*Quantum Electron.*, **34**, 524 (2004)].
18. Kask N.E., Leksina E.G., Michurin S.V. *Kvantovaya Elektron.*, **32**, 437 (2002) [*Quantum Electron.*, **32**, 437 (2002)].
19. Sarychev A.K., Shubin V.A., Shalaev V.M. *Phys. Rev. E*, **59**, 7239 (1999).
20. Heaney M.B. *Phys. Rev. B*, **52**, 12477 (1995)
21. Isichenko M.B. *Rev. Mod. Phys.*, **64**, 961 (1992).
22. Clerc J.P., Giraud G., Laugier J.M., Luck J.M. *Adv. Phys.*, **39**, 191 (1990).